Wear 426–427 (2019) 1222–1232

Contents lists available at ScienceDirect

Wear

journal homepage: www.elsevier.com/locate/wear

Comparison of the sliding wear behaviour of self-mated HIPed Stellite 3 and Stellite 6 in a simulated PWR water environment

Vilma L. Ratia[a,*], Deen Zhang[a], Matthew J. Carrington[a], Jaimie L. Daure[a], D. Graham McCartney[a], Philip H. Shipway[a], David A. Stewart[b]

[a] Faculty of Engineering, University of Nottingham, University Park, Nottingham, United Kingdom
[b] Rolls-Royce plc, Derby, United Kingdom

ARTICLE INFO

Keywords:
Stellite
Cobalt-based alloys
Electron backscatter diffraction
Nuclear
HIP

ABSTRACT

Cobalt-based alloys such as Stellite 3 and Stellite 6 are widely used to protect stainless steel surfaces in primary circuit nuclear reactor applications where high resistance to wear and corrosion are required. In this study, self-mated sliding wear of Stellite 3 and Stellite 6 consolidated by hot isostatic pressing were compared. Tests were performed with a pin-on-disc apparatus enclosed in a water-submerged autoclave environment and wear was measured from room temperature up to 250 °C (a representative pressurized water reactor environment). Both alloys exhibit a microstructure of micron-sized carbides embedded in a cobalt-rich matrix. Stellite 3 (higher tungsten and carbon content) contains M_7C_3 and an eta (η) -carbide whereas Stellite 6 contains only M_7C_3. Furthermore, the former has a significantly higher carbide volume fraction and hardness than the latter. Both alloys show a significant increase in the wear rate as the temperature is increased but Stellite 3 has a higher wear resistance over the entire range; at 250 °C the wear rate of Stellite 6 is more than five times that of Stellite 3. There is only a minimal formation of a transfer layer on the sliding surfaces but electron backscatter diffraction on cross-sections through the wear scar revealed that wear causes partial transformation of the cobalt matrix from fcc to hcp in both alloys over the entire temperature range. It is proposed that the acceleration of wear with increasing temperature in the range studied is associated with a tribocorrosion mechanism and that the higher carbide fraction in Stellite 3 resulted in its reduced wear rate compared to Stellite 6.

1. Introduction

In nuclear steam-raising pressurised water reactor (PWR) plant, the long-term reliability of components is of critical importance. In the PWR primary cooling circuit, the environment is that of high temperature water (typically around 300 °C) of complex chemistry with varying amounts of boric acid, lithium hydroxide and a pH typically above 7. Surface engineering is employed to increase the resistance to wear of certain parts in the primary cooling circuit that are subjected to wear. Because of their excellent combination of resistance to both wear and corrosion, cobalt-based alloys from the Stellite family are extensively used as materials for the hardfacing of valves and other components in the plant. One of the shortcomings of cobalt-based alloys is that cobalt-59 wear debris is carried through the PWR core, and is transmuted by irradiation into its γ-emitting isotope, cobalt-60; this γ-emitting debris is then deposited around the primary circuit and poses a significant health and safety hazard, particularly for those working on maintenance of the plant [1]. This issue has resulted in extensive, largely empirical, research into alternative, low-cobalt hardfacing alloys which have properties at least as good as those of the Stellite family. However, Stellite alloys exhibit some very desirable combinations of properties which have not been readily replicated in candidate replacement materials. Therefore, there is a need for a better fundamental understanding of the wear behaviour of the Stellite family of alloys in the PWR environment to assist with the discovery of improved low-cobalt alternatives.

Two Stellite alloys that are of particular interest for PWR primary circuit applications are Stellite 6 and the less well known alloy Stellite 3. The former is widely used on the sealing surfaces of valves whilst the latter has more limited application in, for example, control rod drive components and other mechanical mechanisms where greater wear resistance is needed.

The cobalt-based alloys which are part of the Stellite family were first developed in the early 1900s and the main grades contain (in addition to cobalt) chromium, tungsten and carbon. The major difference between alloy grades is the carbon and tungsten levels, although

* Corresponding author.
E-mail address: vilma.ratia@nottingham.ac.uk (V.L. Ratia).

https://doi.org/10.1016/j.wear.2019.01.116
Received 30 August 2018; Received in revised form 13 January 2019; Accepted 22 January 2019

control of minor elements such as Fe, Si, Mo, Ni, Mn and B is becoming increasingly important. Chromium has a dual role in the matrix, as a solid solution strengthening element and also in conferring oxidation and corrosion resistance [2]. It also promotes the formation of a metal carbide typically of the M_7C_3 type where M represents normally Cr, Co, Fe. The elements W and Mo contribute to solid solution strengthening of the matrix and, if present in sufficient quantity, promote formation of an eta (η) carbide which has a cubic crystal structure and is typically M_6C or $M_{12}C$ where M is predominantly tungsten. Carbon is necessary for the formation of the metallic carbide phases and increasing carbon concentration in the alloy leads to an increased carbide fraction leading to generally higher hardness at the expense of lower toughness and ductility. The alloys of interest in the present study are Stellite 3 (nominal composition in wt%: Co-30.0 Cr-13.0 W-2.5C plus Ni, Fe, Mn, Si [3]) and Stellite 6 (nominal composition in wt%: Co-28.0 Cr-4.5 W-1.2C plus Mo, Ni, Fe, Si, Mn [4]). The higher carbon level in Stellite 3 results in significantly higher carbide fraction, i.e., ~30-40% in Stellite 3 and ~15% in Stellite 6. One further important feature is that in most Stellite alloys, the cobalt-rich matrix is found to have the face-centred cubic (fcc) crystal structure at room temperature following manufacture by hot isostatic pressing (HIPing). This is a metastable state which has the potential to transform to the stable hexagonal close packed (hcp) structure of the Co-rich solid solution following mechanical deformation [5].

Stellite alloys are used in a number of different forms such as: castings, hot isostatically pressed (HIPed) parts, weld/laser clad overlays and, more recently, hardfacings produced by HIP diffusion bonding of HIP consolidated inserts [6–9]. The manufacturing process greatly affects the microstructure of Stellite alloys which in turn can have a marked influence on wear properties and overall performance [2,10,11]. It is reported that Stellite 3 contains M_7C_3 and M_6C carbides with a volume fraction around 30 vol% which provide this alloy with enhanced wear resistance [2]. However, the microstructural characteristics of HIPed Stellite 3 have not been reported to date. The HIP consolidated form of Stellite 6 has a microstructure comprising a relatively uniform dispersion of M_7C_3 carbides (~15 vol%) [10,12] in a Co-rich matrix of uniform composition; carbides are ~ 1-10 μm in size.

There is a significant body of literature concerning the wear behaviour of Stellite 6, but very little relating to Stellite 3. Moreover, the majority of work relating to Stellite 6 has related to wear in dry conditions (i.e. in an air environment) where the mechanisms of wear are likely to be very different to those operating in the high temperature aqueous environment encountered in a PWR. Given that there is a paucity of literature related directly to wear of materials in conditions representative of the PWR environment, this introduction will seek to summarise relevant literature that addresses wear, corrosion and tribocorrosion of alloys from the Stellite family in the broader context.

1.1. Sliding wear of Stellite alloys

Cobalt alloys are generally regarded as reliable materials for sliding contacts, and this has been argued to be the result of their excellent galling resistance. One factor contributing to the galling resistance of alloys such as Stellite 3 and 6 is the high work hardening ability of the cobalt matrix, in which the metastable face centred cubic (fcc) structure transforms to hexagonally close packed (hcp) structure; it has been demonstrated that this strain induced transformation occurs across the range of temperature up to around 700 °C [5]. Moreover, the resulting hcp structure also has fewer slip systems, which enhances the wear resistance in systems with contact between metal surfaces. It has been argued that this fcc to hcp phase transformation (rather than the overall alloy hardness or the volume fraction of hard phases) plays the most significant role in conferring wear resistance to these materials [7].

The low stacking fault energy (SFE) is also often cited as an underlying factor in the excellent sliding wear resistance of cobalt alloys, in that this limits dislocation cross-slip and climb. Bhansali and Miller [13] compared alloys with cobalt and nickel matrices and attributed the galling resistance of the cobalt-based systems to their low SFE. Crook and Li [14] examined the behaviour of cobalt-chromium alloys and linked a reduction in resistance to wear with increasing temperature to changes in the SFE. However, they also observed that with continued increase in temperature (above 250 °C), the wear resistance then increased, associated with the formation of a protective glaze layer when exposed at these temperatures in an air atmosphere, with similar observations being made by Stott et al. [15].

The tribological damage occurring in Stellite 6 and Stellite 21 (a Stellite with low carbide content [16]) under dry sliding conditions was studied by Persson and co workers [16–18], who concluded that the alloys form several layers during wear: an oxide layer, an thin easy-shear layer and a thicker work hardened layer. They concluded that the preferentially oriented, easily sheared superficial layer (hcp cobalt basal planes) was the most significant in conferring wear resistance.

In summary, it can be concluded that wear in Stellite alloys is affected by a combination of several factors including: the carbide content and morphology [10]; the strain induced fcc to hcp transformation of the Co-matrix [7]; and, at elevated temperature, the formation of a protective oxide layer [14,15].

1.2. Aqueous corrosion of Stellite alloys

Corrosion behaviour of cobalt alloys in PWR-simulating conditions has been studied by several authors; tests are typically conducted at high temperature (up to ~ 300 °C) and high pressure with water of low oxygen content with additions of LiOH (for pH control) or, in some cases, a combination of LiOH and H_3BO_3 (the latter being added in service as a neutron absorber). Oxide films are observed to be enriched in chromium but depleted in cobalt and their growth is believed to result from solid state diffusion and preferential dissolution of cobalt from the oxide-solution interface [19–23]. Thicker oxide layers are typically observed on the matrix material than on the carbides [23]. In addition, Karimi et al. [24] (who conducted exposure tests on a Stellite 3 analogue) observed interfacial corrosion between the chromium-rich carbides and the cobalt-rich matrix, which they attributed to an electrochemical effect.

Both the mechanisms and the rate of corrosion of alloys in these conditions are sensitive to temperature. Taylor and Armson [22] studied the cobalt release rates in cobalt alloys and observed that they were approximately ten times higher at 250 °C than at 180 °C, but that a further increase in temperature to 290 °C did not result in further increases of such significance.

1.3. Tribocorrosion of Stellite alloys

Wear is influenced by both the mechanical and environmental conditions of the tribosystem, and due to the complex interactions between these, they must be considered together. Tribocorrosion in Stellite alloys when exposed to PWR conditions is associated with material loss through mechanical damage alongside the growth of passivating oxide layers, and their subsequent mechanical removal through wear [25,26]. The differences between laboratory loop studies and the actual behaviour of Stellite 6 in PWR trials (control rod drive mechanisms) was attributed to tribocorrosion effects by Lemaire and Calvar [27]. Under ambient temperature, Guadalupe Maldonado et al. [28] studied the tribocorrosion of Stellite 21 type CoCrMo alloy using a H_2SO_4 solution under a range of conditions. They reported wear to increase when a passive film forms on the surface, and film formation was found to increase the mechanical wear by about an order of magnitude (i.e. corrosion accelerated by wear).

The effect of wear on the corrosion rate in PWR-simulating conditions was directly demonstrated by Xu et al. [29], who conducted electrochemical measurements of the rate of corrosion in UNS R30006 (a Stellite 6 type alloy) before and after subjecting the surface to sliding

wear. A contact under a relatively small nominal stress of 1.4 kPa was used to disrupt the oxide layers in the interface. It was observed that the corrosion rate did not substantially increase after the wear event (which removed the passive films) at low (25–65 °C) temperatures, but that corrosion was significantly enhanced at higher (150–250 °C) temperatures; at these temperatures, the increase could be eight fold in comparison to the corrosion rate prior to the wear event (depending upon the specific conditions), and it took up to around 20 min before the corrosion rate had returned to the levels prior to the wear event. Recently, the present authors studied the temperature dependence of wear in Stellite 6 in representative PWR conditions [30]. It was found that the wear increased markedly above 150 °C and it was proposed that this is mainly due to a tribocorrosion effect, specifically to increasing corrosion rate with increasing temperature and the removal of corrosion product from the surface during wear.

1.4. Aims of this work

As already argued, in seeking to find low-cobalt alternatives to replace Stellites in PWR applications, there is a need for a fundamental understanding of the wear behaviour of the Stellites themselves under such conditions. The aim of the present study is to extend our previous work on Stellite 6 in order to understand how Stellite alloys with different volume fractions of hard phase particles behave under tribocorrosion conditions. Specifically, this paper will report work undertaken to characterize and compare the wear rates and mechanisms of self-mated Stellite 3 and Stellite 6 (both in the HIPed condition) tested in a simulated PWR environment over a range of temperatures so as to gain insight into the role of hard particle type and volume fraction on material damage and mechanisms.

2. Materials and methods

2.1. Materials

The materials examined in this work were the cobalt alloys Stellite 3 and Stellite 6 which had been manufactured by hot isostatic pressing (HIPing) and supplied by LSN Diffusion (Llandybie, UK). Table 1 presents the compositional analysis of the two materials, the analyses having been conducted by AMG Analytical Services (Rotherham, UK).

2.2. Autoclave wear testing

Wear testing was conducted with a pin-on-disc apparatus placed in an autoclave, which allowed testing in an elevated temperature, elevated pressure aqueous environment. The test was conducted as same-pair material tests, i.e. the pin and the disc within the test being the same material stock. Fig. 1 shows the test setup, which comprises a disc of 30 mm diameter (with a ground surface, Ra ~0.4 μm) mounted in a rotating sample holder, and a pin with 10 mm diameter with a 50 mm radius spherical cap having been ground onto the end face in contact. The pin is loaded against the rotating disc via a 4 kg stainless steel dead weight. The load is stabilised with a mechanism that allows free vertical movement of the load. As the dead loading system is submerged in water, buoyancy effects result in small changes in contact load; the changes in the densities of both the water and the steel across the temperature range employed cause the contact force to vary between ~ 35 and 37 N.

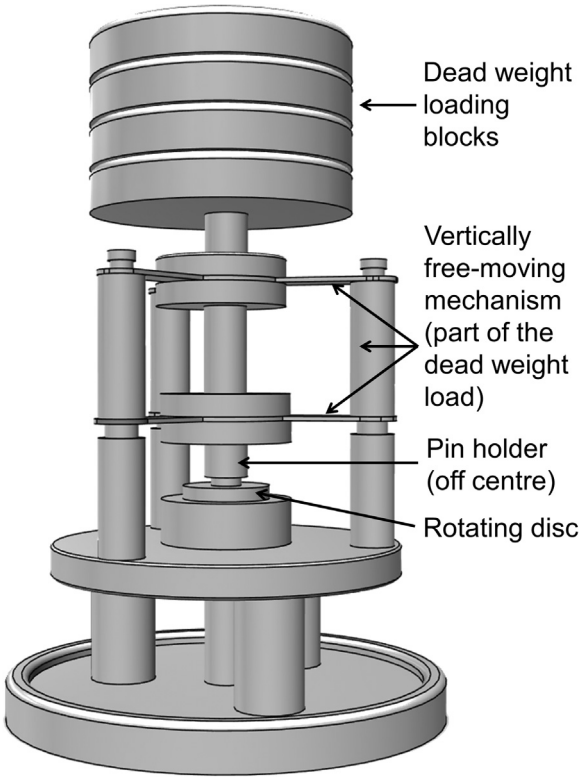

Fig. 1. Schematic diagram of the pin-on-disc wear testing apparatus which was enclosed in an autoclave [30].

Deoxygenated deionised water was used as the testing media, with an addition of 8.5 mg of LiOH per litre which resulted in the solution having a pH of approximately 10.5 at room temperature when prepared. The concentration of boric acid is known to vary during PWR plant operation, and so to eliminate this effect, no boric acid was added to the solution in our study. Several water temperatures (measured via a thermowell placed inside the autoclave) were used for tests as follows: room temperature (~ 20 °C), 80 °C, 150 °C, 200 °C and 250 °C. The pressure in the system was built up autogenously (i.e. there was no external pressurisation employed). A constant value of 200 rpm was employed for the rotation of the disc, which is driven through a magnetic coupling with an external drive. There is a 10 mm offset between the axis of loading and the axis of rotation, resulting in a wear track diameter of 20 mm and sliding speed of 0.21 m s^{-1} in the centre of the track. Two test durations (either 5 or 24 h) were used, corresponding to approximate sliding distances of 3 770 and 18 100 m, respectively. The different testing durations were required since Stellite 3 and 6 exhibited very different mass losses over the range of test temperatures examined. Longer test times were selected for Stellite 3 to achieve readily measurable mass losses whereas shorter test times were needed for Stellite 6 to ensure that during a single test, the spherical cap of the wear pin was not completely removed.

Normally, two tests were conducted under each set of testing conditions. The wear of both the pin and disc was measured by mass loss to a precision of 0.1 mg. Profilometry was carried out on the disc samples to verify the trends seen in mass losses.

To measure the effect of the mass change arising from corrosion during a test, an exposure test of a disc sample in deoxygenated lithiated water was conducted without applying sliding contact at 250 °C for

Table 1
Chemical compositions of HIPed Stellite 3 and 6 in wt% as determined by inductively coupled plasma analysis except for carbon which was determined by combustion infrared detection.

Alloy	Element [wt%]								
	Co	Cr	Fe	Ni	Si	W	C	Mn	Mo
Stellite 3[a]	bal.	29.57	2.32	1.07	1.79	12.07	2.52	0.75	0.67
Stellite 6[b]	bal.	27.08	0.73	0.87	1.47	5.01	0.96	0.07	–

[a] also included Cu, Nb, Ti, V < 0.1 wt%.
[b] also included Cu < 0.1 wt%.

24 h. During the test, the disc was mounted into the disc holder and it was rotated as in a wear test, but without contact of the pin. Heating of the system from room temperature to 250 °C took about 5.5 h, and after reaching 250 °C, the sample was held at the temperature for 24 h. After that the system was allowed to cool down, which took up to 17 h.

2.3. Materials characterisation

A Vickers hardness tester with 20 kgf (196 N) load was used for determining the macrohardness of the alloys. The reported values are an average of 20–25 measurements for each material.

Microstructures, the worn surfaces of both the pin and the disc, and the wear debris were examined with a JEOL 6490LV scanning electron microscope (SEM), using both secondary electron (SE) and back-scattered electron (BSE) imaging. Energy dispersive X-ray analysis (EDX) was used in identifying the composition of any features of interest. A JEOL 7100F field emission gun SEM (FEG-SEM) was used for more detailed analysis of the worn samples. Electron backscatter diffraction (EBSD) was utilised to obtain information regarding changes in phase proportions and grain orientations in the materials following wear. For EBSD, an accelerating voltage of 15 kV and a step size of 0.06 μm (for wear scar cross-sections) or 0.10 μm (for bulk material) were used, along with Aztec software for acquisition. The volume fraction of carbides was measured from BSE images using ImageJ software [31].

X-ray diffraction (XRD) was used for determining the phase make-up of the alloys and in the wear tracks. A Bruker D500 diffractometer with monochromatic Cu-Kα radiation was used for large area analysis, parameters being 40 kV for tube voltage and 25 mA for tube current, a step size of 0.01° and a step dwell time of 7 s. For point source XRD (where diffraction information is gathered from an area with the maximum length of up to ~2.5 mm), a Bruker-AXS D8 Discover with Cr-Kα radiation was used, the parameters being 30 kV for tube voltage and 35 mA for tube current, a step size of 0.04° and a step dwell time of 15 s.

Profilometry was conducted on the wear scars of the discs to allow both the wear depth and the volume loss to be estimated, the latter allowing a comparison with the mass loss data to be made. A Taylor Hobson Form 50 Talysurf stylus profilometer was used, and typically four profiles were obtained across the wear scars of a representative worn disc tested at each condition (temperature / test duration combination). The wear volume can be estimated from the average cross-sectional area of the track.

3. Results

3.1. Materials characterisation

Fig. 2 presents the XRD patterns of both of the materials in the polished state. The XRD pattern of Stellite 3 (Fig. 2a) shows that the HIPed alloy is predominantly face centred cubic cobalt solid solution. There are additional peaks which can be indexed to two distinct carbide phases: an M_7C_3 carbide and η-carbide (M_6C or $M_{12}C$). The Stellite 6 pattern (Fig. 2b) shows that the material consists of a cobalt-rich matrix with predominantly face centred cubic structure and an M_7C_3 carbide.

Fig. 3 presents the SEM images of cross sections, taken in BSE mode, and EBSD phase maps for both of the materials. In Stellite 3 (Fig. 3a), three main phases can be clearly identified in the BSE images: a light grey matrix phase identified as the cobalt rich matrix phase (containing also chromium, tungsten, iron and silicon in solution) and two kinds of precipitates. The bright precipitate was found by EDX analysis to contain significantly (about ten-fold) more tungsten than the surrounding phases and can be identified as the η-carbide. The dark precipitate was found to be chromium-rich and is evidently the M_7C_3 type carbide.

The EBSD derived phase map (Fig. 3c) supports the identification of the three main phases seen as blue (fcc cobalt; for greyscale image colours see the phase key in the bottom of the image), yellow (chromium-rich M_7C_3 carbide) and green (tungsten-rich η-carbide). In the matrix, there are also small regions of cobalt with the hcp structure (red), possibly resulting from sample preparation damage [30]. Image analysis revealed the carbide content to be approximately 24 ± 1 vol% for the M_7C_3 carbides and 18 ± 1 vol% for the η-carbide. The macrohardness of Stellite 3 was 655 ± 8 HV20.

Stellite 6 (Fig. 3b) has a cobalt-rich matrix (with chromium, tungsten, iron and silicon in solid solution) and the dark precipitates, chromium-rich in composition, are evidently M_7C_3. The EBSD-derived phase map (Fig. 3d) confirms this, with the fcc cobalt seen as blue, and chromium-rich M_7C_3 carbide seen as yellow. Small areas of the cobalt-rich matrix with an hcp structure (marked with red) can also be seen. Image analysis revealed the carbide content to be approximately

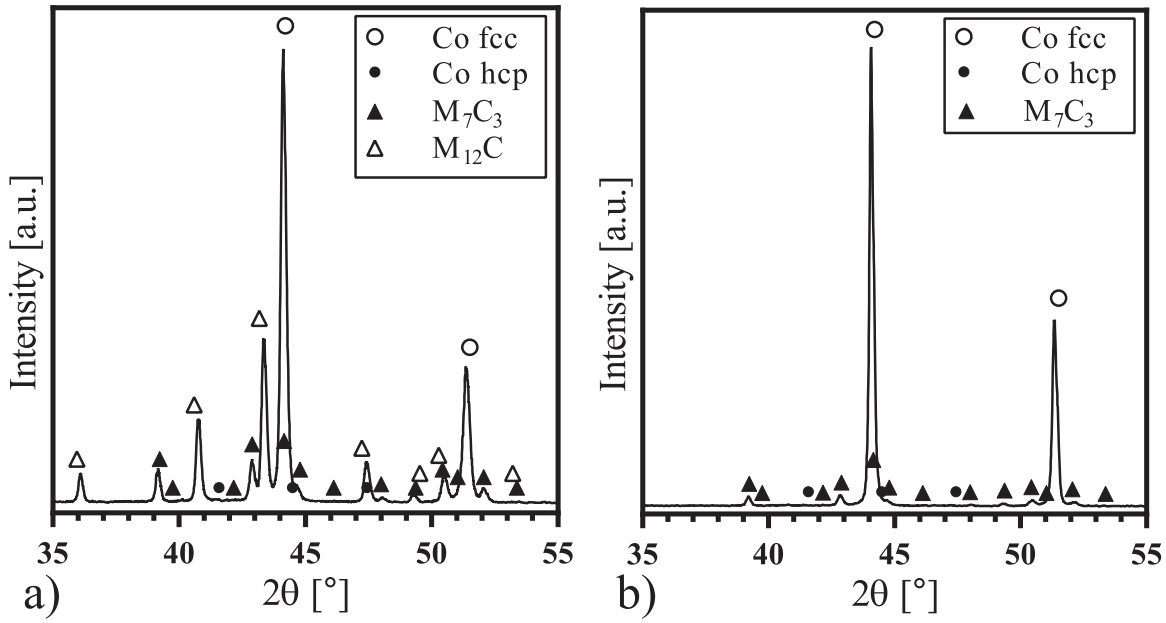

Fig. 2. XRD patterns obtained from the polished surfaces of HIPed material a) Stellite 3 and b) Stellite 6. The results for Stellite 6 have been presented previously in [30].

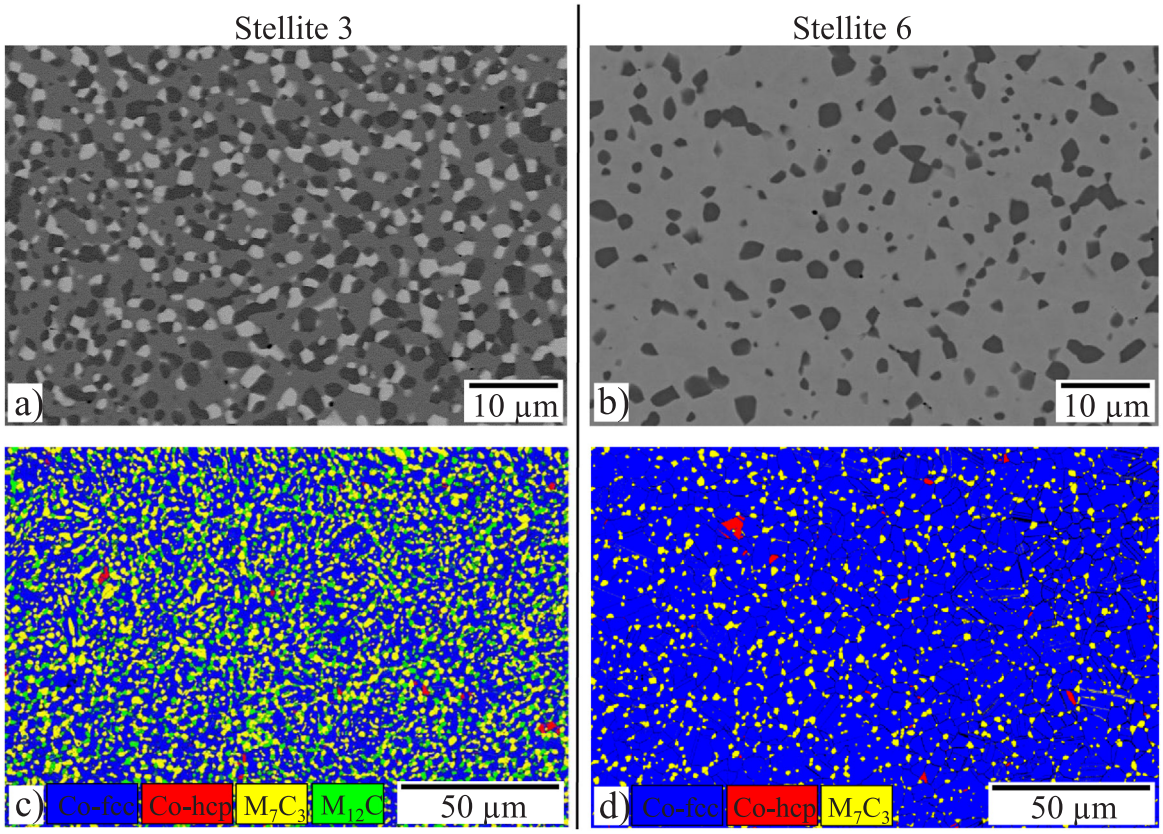

Fig. 3. BSE images (a, b) and EBSD derived phase maps (c, d) of the polished bulk microstructures of HIPed Stellite 3 (a, c) and Stellite 6 (b, d).

13 ± 2 vol%. The macrohardness of Stellite 6 was 400 ± 2 HV20.

3.2. Wear test results

3.2.1. Mass loss

Fig. 4 presents the mass loss values for both the alloys. The plots include results for 5 and 24 h duration tests and data are shown separately for the mass losses of the pin and the disc along with the combined mass loss.

During the wear testing of Stellite 3 (Fig. 4a), only superficial wear was observed following 5 h testing at the lower temperatures. Therefore, the majority of the testing for Stellite 3 was conducted for 24 h, whereas the testing for Stellite 6 (Fig. 4b) was conducted mainly with the 5 h test duration because of its greater wear rate.

The mass loss recorded for Stellite 3 is much lower than for Stellite 6. For example, at 250 °C, the mass loss for Stellite 3 is only around one fifth that of Stellite 6 for 5 h duration. This is not unexpected, as the hardness of Stellite 3 is significantly greater and it has a significantly

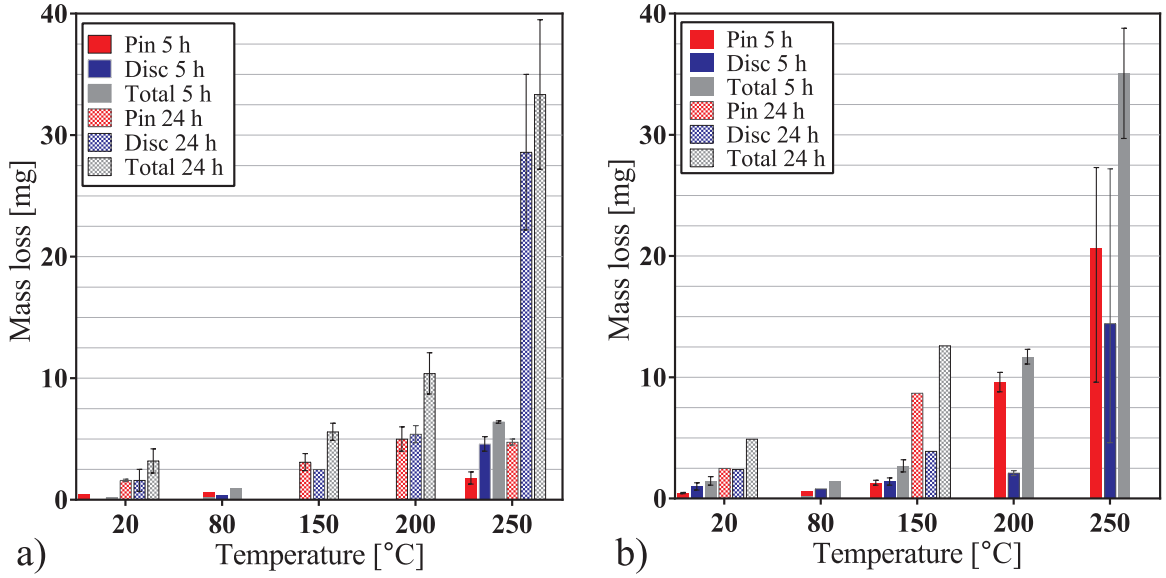

Fig. 4. Average mass loss results from the wear tests at a range of temperatures for a) Stellite 3 and b) Stellite 6. The error bars represent the minimum and maximum values. Solid bars are for the 5 h tests and hatched bars for the 24 h tests. The results for Stellite 6 have been presented previously [30].

higher carbide volume fraction. At lower temperatures, the 24 h tests revealed the wear in Stellite 3 to be approximately one half that of the Stellite 6. A transition in mass loss appears to occur in both alloys above approximately 150 °C. They both undergo a very significant increase in wear rate, especially above 200 °C. In Stellite 6, this transition seems to be a bit more pronounced, a steeper increase occurring after 150 °C than in Stellite 3, where the increase is more gradual between 150 and 250 °C. In both materials, the effect of the temperature on the mass loss is significant.

When considering Stellite 3, the tests at 250 °C for 5 and 24 h show that the rate of mass loss is actually rather similar for both of the test durations, being approximately 1.3–1.4 mg/h for the total wear. For both of these durations, the disc wear clearly exceeded the wear of the pin. For the longer test, this was more evident, the disc wearing approximately six times more than the pin at 250 °C. The differences in the pin and the disc mass loss is more apparent above 200 °C in Stellite 3 whilst below 200 °C, the pin and the disc are wearing approximately the same amount. In the case of Stellite 6, pin wear tended to exceed disc wear at elevated temperature.

Mass loss by corrosion was investigated by conducting 24 h tests at 250 °C on disc samples without mechanical loading. The mass change of the disc in both of the alloys was less than 0.2 mg, so it can be seen that this is negligible compared to that resulting from wear and/or tribo-corrosion.

3.2.2. Wear scar profiles

Mass loss measurements are affected by changes in the entire sample, so the trends seen in the mass loss measurements were verified with profilometry. Fig. 5 presents the profiles across the wear scars on the discs, for the 24 h tests for Stellite 3 (Fig. 5a) and for the 5 h tests for Stellite 6 (Fig. 5b). They confirm the mass loss results, the wear scar being significantly shallower at lower temperatures in both materials. Furthermore, maximum wear scar depths of Stellite 6 after 5 h wear duration are comparable to those in Stellite 3 after 24 h duration at the test temperatures examined.

3.3. Characterisation of wear surface and features

An increase in the discolouration of the sample surfaces was observed with increasing temperature, indicating increased thickness of the corrosion film formed generally across the surface. Samples tested at both 200 and 250 °C exhibited distinct discolouration due to corrosion film formation in Stellite 3. The wear scars on the discs reveal that as the temperature increased, light scoring progressed into deeper and wider wear scars.

Different regions can be identified within the wear scars, especially at higher temperatures. Areas with scoring are accompanied by areas having oxide scales, as observed in Fig. 6b and c. When comparing Stellite 3 samples from tests that were run at 250 °C for both 5 h and 24 h, the prevalence of regions with oxide scale was observed to decrease with test duration. Oxide areas are more frequently observed in the samples following the shorter test duration of 5 h, or on the outer region of the pin wear surface. Also, local smeared areas with contrast similar to that of the matrix material are observed on the wear track (Fig. 6b and c).

Fig. 6a-c show SEM images of the wear scars on the Stellite 3 pins following wear for 24 h at 20 °C, 200 °C and 250 °C. Wear surfaces of Stellite 3 revealed oxide formation, scoring, local matrix removal and scratching. Fig. 6d-f show the plan view of Stellite 6 tested at 20, 200 and 250 °C for 5 h. In macroscale, in the shorter tests at low temperatures the wear scar has not penetrated through the grinding marks in all of its length. At 250 °C, however, more significant wear is observed as deeper and more frequent scratches. No clear debris layer was found to form at any of the tested temperatures, although some oxidation and debris accumulation can be seen on the surface, observed as dark areas in Fig. 6e. Also pull-out of the carbides appeared to occur. However, most of the wear surface could be characterised as relatively flat with rather light scoring through both of the matrix and the carbide hard phase, there being no major change between the temperatures for the mechanisms. The wear scars contained several different areas, which could be found across the tested temperatures; these area types were oxidised areas, carbide pull-out, scratching (at times possibly due to carbide pull-out) and smoother scored areas [30]. The presence of oxide debris accumulated in original grinding marks is more significant at temperatures above 20 °C, and they tend to be found toward the outskirts of the wear scars in the discs.

In the case of Stellite 3, the matrix seemed to be removed preferentially in some locations, as in Fig. 7a, where the matrix seems to have worn away, leaving carbides protruding from the surface. Locally, there are areas that have been affected more heavily than the surrounding areas, as seen in Fig. 7b. These areas have heavier oxide formation, and the matrix is often removed from around the carbides. This type of attacked area was more frequently observed in the Stellite 3 than in Stellite 6. In most of the areas though, the matrix and the

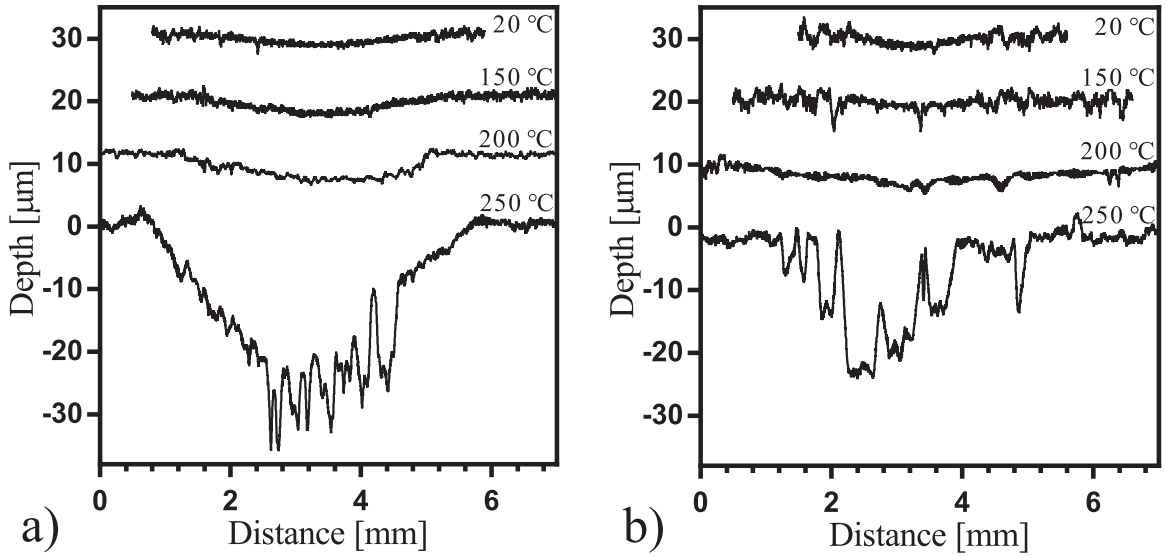

Fig. 5. Cross section profiles of disc wear scars in samples tested at 20, 150, 200 and 250 °C: a) Stellite 3 tested for 24 h and b) Stellite 6 tested for 5 h. The results for Stellite 6 have been previously presented in [30].

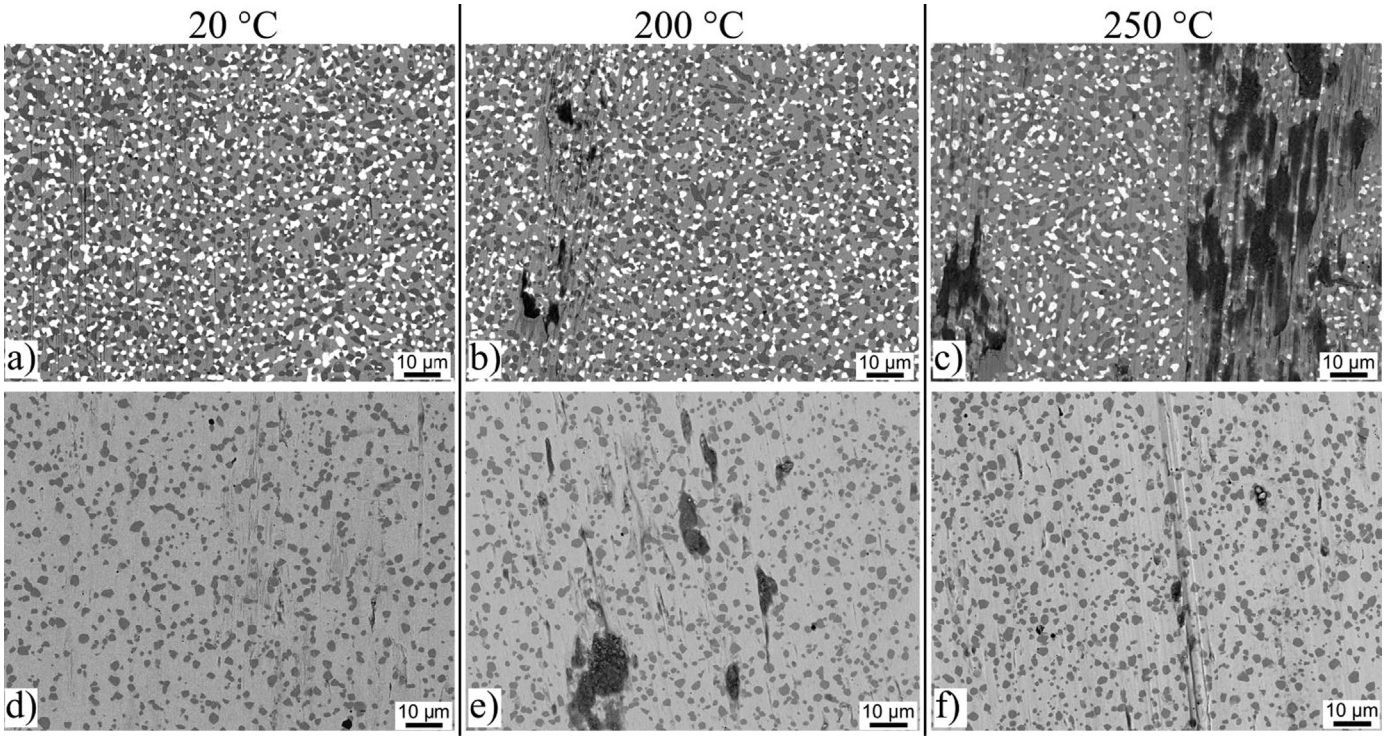

Fig. 6. Plan view SEM/BSE micrographs of the wear scars on pin samples following testing of Stellite 3 for 24 h (a-c) and Stellite 6 for 5 h (d-f). Test temperature was 20 °C (a, d), 200 °C (b, e) or 250 °C (c, f).

carbides appear to wear at the same rate, shallow scratches extending across both of them as seen on the left hand side in Fig. 7c (the grey contrast is the matrix and the features with darker and lighter contrast are the M_7C_3 and η carbides respectively). However, pull-out sites were also observed, as depicted in the middle of the same image.

3.4. Characterisation of wear track phases and microstructure

Point source XRD was conducted on the worn discs both predominantly inside and outside the wear track to indicate in a semi-quantitative way the fcc to hcp transformation which had taken place in sub-surface regions during wear. The diffractograms are presented in Fig. 8 and show the XRD patterns for both alloys, in the 2θ range of 70–85° with Cr-Kα radiation (corresponding to the 2θ range 45.4–54.1° with Cu-Kα radiation). This range contains the cobalt peaks not overlapping with carbide peaks in Stellite 6; with Stellite 3, the peak at around 73.5° overlaps with only a minor peak from the η-carbide. The X-ray patterns originate from a depth within the sample of ~ 20 μm but the major proportion is from the top few microns.

From all three XRD patterns in Fig. 8, it is clear that there was some hcp matrix phase present already in the unworn surface, due to the grinding process in sample preparation. This has been noted previously in Stellites [30,32]. Fig. 8a presents the patterns obtained from Stellite 3 samples tested at 20 °C for 5 and 24 h. The duration of the wear seemed to cause only a rather small difference in the relative peak heights which is a semi-quantitative measure of the degree of transformation. This is an interesting observation, as in Stellite 6, longer testing seemed to lead to higher degree of transformation as found in a previous study [30]. The similar extent of transformation for different durations may be originating from the higher carbide content of Stellite 3, which provides more mechanical support to the matrix and does not facilitate the transformation to such depths when compared to Stellite 6. Fig. 8b shows the point source XRD patterns of Stellite 3 for different testing temperatures. The degree of transformation in Stellite 3 seemed to be slightly higher at 250 °C than at 20 °C as judged by the relative peak heights of fcc to hcp. Fig. 8c shows the patterns obtained from Stellite 6 tested for 5 h at 20 °C and 250 °C. These reveal little effect of temperature on transformation within the area and penetration depth analysed.

In light of the XRD evidence, electron backscatter diffraction (EBSD) was used to investigate the extent of the fcc to hcp phase transformation immediately below the worn surface. Fig. 9 shows EBSD-derived band

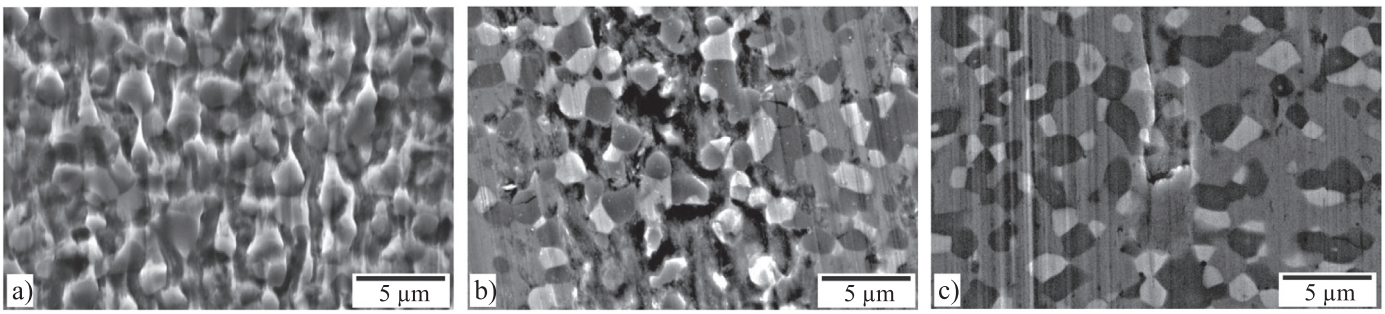

Fig. 7. SEM/SE images of wear scar details in Stellite 3 showing a) worn away matrix exposing the carbide skeleton (in disc tested at 20 °C for 24 h), b) matrix degradation with oxidation (in pin tested at 250 °C for 5 h) and c) scoring and carbide pull-out (in disc tested at 250 °C for 24 h).

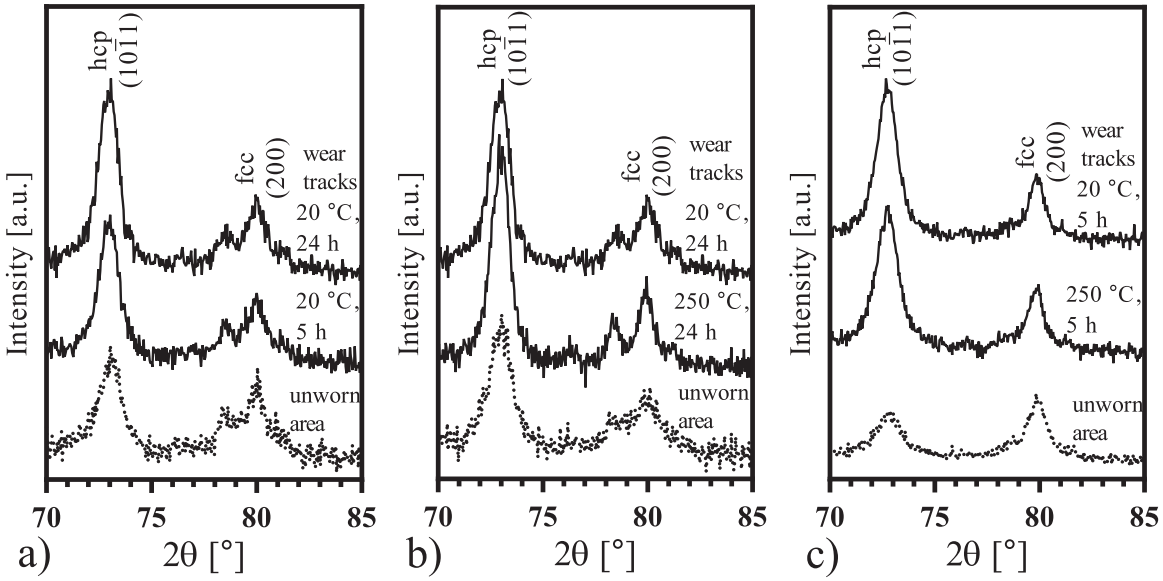

Fig. 8. Point source XRD patterns of wear tracks and unworn area in a) Stellite 3 tested at 20 °C for 5 and 24 h, b) Stellite 3 tested at 20 °C and 250 °C for 24 h and c) Stellite 6 tested at 20 °C and 250 °C for 5 h, obtained with Cr-Kα radiation. The Stellite 6 results have been previously published in [30].

contrast images and phase maps obtained from cross-sections through ground surfaces (prior to any wear) of both Stellite 3 and Stellite 6. It can be seen that the immediate subsurface is damaged by grinding, which is indicated by the presence of unindexed areas shown as black pixels in Fig. 9c and d. Some localised phase transformation is also occurring, with the fcc cobalt matrix (blue; for greyscale image colours see the phase key in the bottom of the image) being locally transformed to hcp cobalt (red). Transformation twinning of the matrix is also clearly seen in the band contrast images.

In Fig. 10, sub-surface sections through wear tracks following testing at 20 °C are presented. In the Stellite 3 sample, the degree of damage appears to be smaller than in Stellite 6, as shown by comparison of Fig. 10c and d. This may be due to an almost burnishing type of wear at low temperature in this alloy with the higher carbide volume fraction. The matrix transformation to an hcp structure (shown as red in the phasemaps) typically seems to occur almost completely to a depth of approximately 2 μm, with a small degree of transformation occurring to a depth of about 10–15 μm below the wearing surface. The transformation is often localised close to carbide-matrix interfaces, possibly due to stress accumulation due to differences in deformation behaviour between the matrix and carbide phases.

When comparing Stellite 3 with Stellite 6, the layer which has

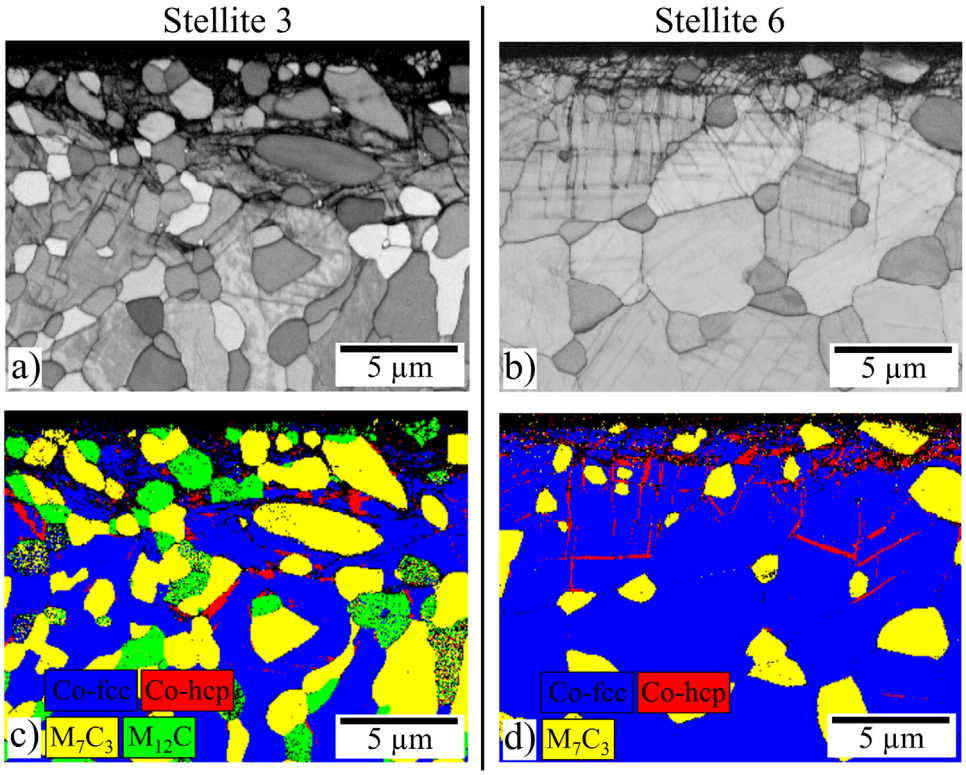

Fig. 9. EBSD derived band contrast images (a, b) and phase maps (c, d) of cross sections through a ground surface without wear. Stellite 3 (a, c) and Stellite 6 (b, d).

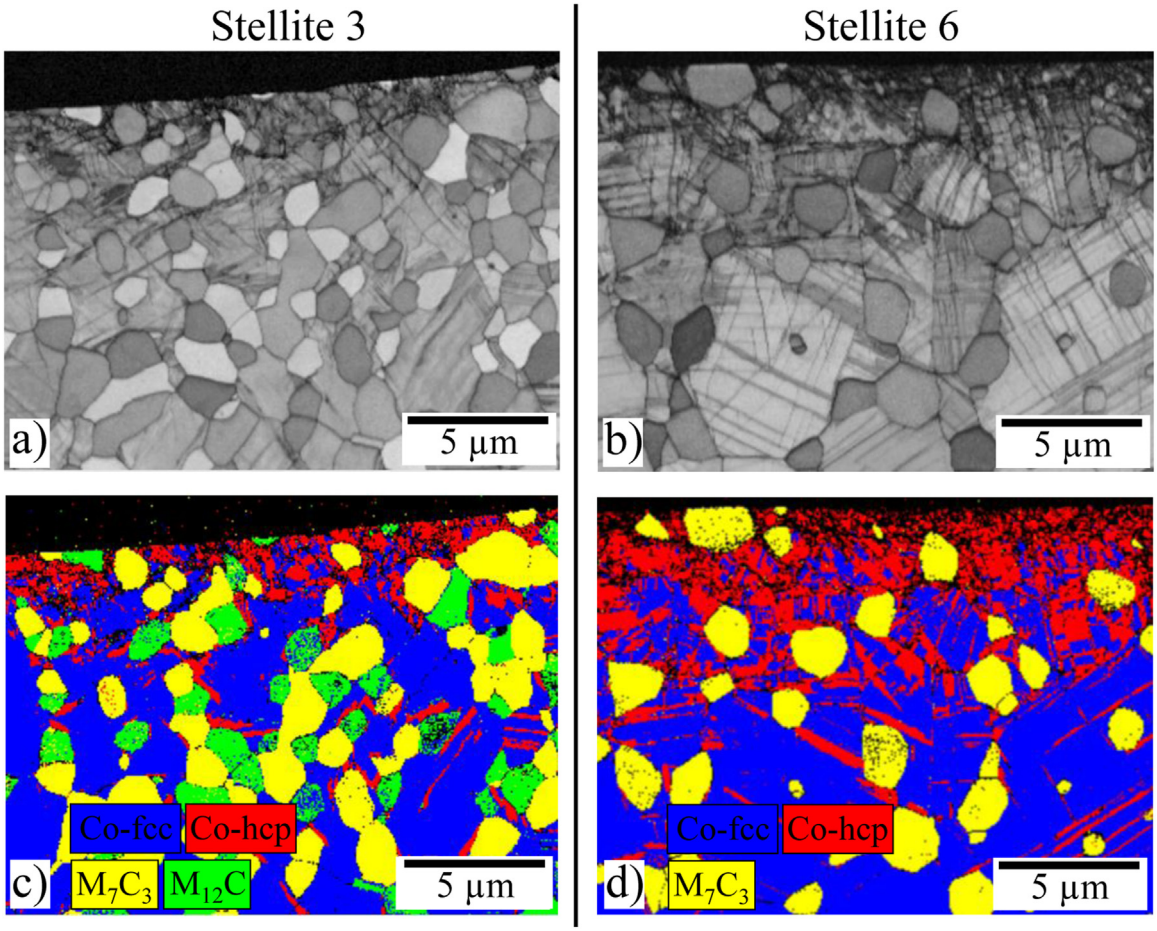

Fig. 10. EBSD derived band contrast images (a, b) and phase maps (c, d) of cross sections through a wear scar region following testing for 24 h at 20 °C. Stellite 3 (a, c) and Stellite 6 (b, d).

undergone almost complete transformation from fcc to hcp cobalt extends further below the wearing surface in Stellite 6. This is probably due to the lower amount of hard phase, and larger mean free path in the matrix carrying the load in Stellite 6. Thus, there is a greater degree of matrix deformation and the subsequent phase transformation. The deformation of the matrix appears to generate twinning in addition to the fcc to hcp transformation as seen in the band contrast images of Fig. 10a and b.

3.5. Wear debris

Loose debris was collected following the tests from the top of the wear discs, and BSE images of such debris from Stellite 3 and Stellite 6 wear tests at 250 °C are shown in Fig. 11. The debris collected from the Stellite 3 tests at the lower temperature of 20 °C was composed of agglomerates of very fine particles. Following tests at 250 °C, the debris is composed of larger angular particles with the size of up to a few microns (Fig. 11a). Some of the particles are rich in tungsten (the bright contrast particles), as confirmed by EDX. This observation, along with the bright particle size being approximately 3–5 µm, suggests that some carbides are removed from the wearing surface during testing at 250 °C.

For Stellite 6, the debris from tests at 20 °C is again mostly very fine, although some agglomerates of fine particles were observed. Following wear at 250 °C (Fig. 11b), the wear debris also contained coarser particles than those seen after wear at 20 °C, and the agglomerates were generally larger and more prevalent.

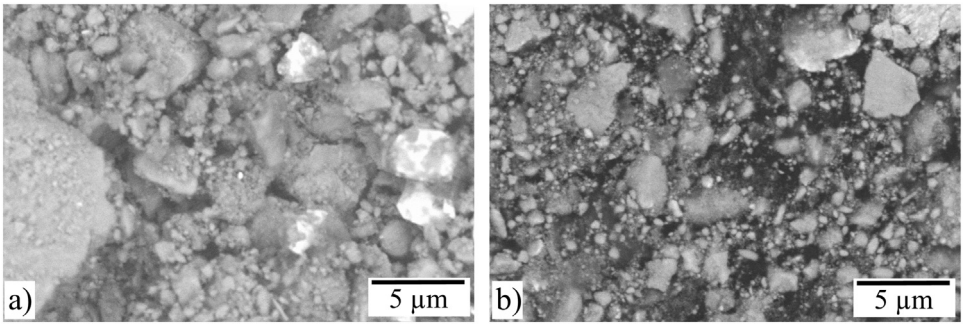

Fig. 11. BSE images of wear debris collected after testing at 250 °C: a) Stellite 3 (24 h) and b) Stellite 6 (5 h).

4. Discussion

To summarise the main differences between the two Stellite materials: i) the higher carbon content in Stellite 3 leads to higher volume fraction of carbides in comparison to Stellite 6 – the overall volume fractions being approximately 42 and 13 vol%, respectively; ii) the higher carbide content results in considerably higher hardness of Stellite 3 than Stellite 6 – 655 ± 8 and 400 ± 2 HV20, respectively and iii) there being two different main carbide species in Stellite 3 (M_7C_3 and η-carbide), whereas the carbides in Stellite 6 are single species, M_7C_3.

Despite their differences, the behaviour of the two materials is similar in many ways. They both show a rather rapid increase of wear with temperature above 150–200 °C, and wear takes place through scoring, carbide pull-out and formation of oxides. Moreover, they both exhibit the fcc-to-hcp cobalt matrix transformation across the whole temperature range.

However, there are some differences as well: Stellite 6 wears significantly more, the difference being about five fold in mass loss at 250 °C in the 5 h test. Looking into the wear mechanisms in more detail, Stellite 3 appears to be more susceptible to localised attacks on matrix, these areas having the matrix worn away and often associated with debris accumulation. Another difference between the matrix behaviour is the lower degree of deformation seen in the Stellite 3 matrix in comparison to Stellite 6 in similar testing conditions.

4.1. Role of carbide volume fraction and carbide type

One of the most obvious effects of the three fold higher carbide content of Stellite 3 is its significantly higher hardness in comparison to Stellite 6, the average hardness values being 655 and 400 HV20, respectively. This, in turn, manifests itself as better wear resistance of Stellite 3.

In addition to different carbide content, also the carbides themselves are different: Stellite 3 includes two kinds of carbides – the chromium rich carbides and the tungsten rich carbides. Stellite 6 has one type of carbide, which is chromium rich.

For Stellite 6, the hardness at high temperature is reported to be approximately 15–20% lower at 250 °C than at room temperature, and the decrease is rather linear [33,34]. Kapoor et al. [35] previously described the chromium-rich carbide as undergoing a much smaller decrease in hardness in comparison to the matrix; however, their measurements were divided to matrix-only and carbide-and-matrix types, and thus the carbide was not measured exclusively. Yamamoto et al. [36] conducted measurements of M_7C_3 type carbides with varying levels of tungsten (in cast iron) and found the carbide hardness to decrease in the range of 20% when raising the temperature up to about 300 °C. For the η carbide, hardness data is much more challenging to find. Liu et al. [37] did measure some elevated temperature hardness on cobalt based alloys with carbides they recognised as $(W,Co)_6M$/Co_4W_2M type carbides. They reported only a subtle change in hardness between the room temperature and 250 °C, difference being less than 20 HV. They measured some M_7C_3 type carbide hardness as well, concluding that the M_7C_3 carbide is harder.

The volume fraction also seems to have an effect on the work hardening ability of the material: Stellite 3 has lower amount of cobalt matrix and also more supporting carbides to distribute the load, and this results in a lesser degree of matrix phase transformation from fcc to hcp than observed in the Stelllite 6. It may be that the smaller effect of sliding distance is due to the higher support by carbides as well.

It is interesting, though, that Stellite 3 appeared to experience a slightly higher degree of phase transformation at higher temperature. Even though the reduction of carbide hardness is not large, it might facilitate a slightly higher degree of phase transformation.

4.2. Role of corrosion and tribocorrosion

It seems unlikely that the wear increases steeply at high temperatures due to hardness reduction or change in transformation induced work hardening behaviour. Therefore the role of tribocorrosion must be considered. Tribocorrosion accelerates the wear through the repetitive removal of formed corrosion films, which exposes new material to be corroded at a rate faster than that at which it can form a protective layer. In the previous study on Stellite 6 [30], the steep increase of wear at above 150 °C was proposed to be mainly due to tribocorrosion.

Lemaire and Le Calvar [27] concluded tribocorrosion to be the reason why there was a mismatch between the field tests and the laboratory tests in PWR conditions, field samples wearing considerably more. They stated that latency time (that is, the time between contacts) was important – a longer time between the contacts would allow thicker corrosion film to be formed, and thus more material would be removed when contact took place. With regard to this theory, the pin and the disc samples in the current autoclave sliding test experience very different latency times: the pin, which is always in contact with the counterpart, and the disc, which is in contact with the pin only once every 0.3 s in a certain location. For Stellite 3, the difference between the samples can indeed be seen, the disc wearing substantially more at 250 °C, possibly due to longer latency time.

Karimi et al. [24] studied the corrosion of a cast Stellite 3 analogue in simulated PWR conditions after 30 day exposure and found that there was interfacial corrosion between the chromium rich carbide and cobalt matrix, but not between the tungsten rich carbide and matrix. This was proposed to be due to higher electrical potential between the M_7C_3 type carbide and matrix. Preferential corrosion cannot be seen in the current Stellite 3 samples at any temperatures, but it must be considered that the period of exposure is much shorter in the current test than the tests of Karimi et al. However, such findings could suggest that Stellite 3 type matrix can be prone to corrosion effects when exposed to lithiated high temperature water.

When considering both Stellite 3 and 6, it can be seen that on one hand, the increase of wear occurs at above 150 °C, and on the other hand the main wear mechanisms and work hardening remain similar across the temperatures for both materials. Thus, it is proposed that the main factor causing the increase both of the materials at higher temperatures is the phenomenon of tribocorrosion.

5. Conclusions

In this study, two HIPed Stellite alloys with different carbide fraction were tested for their sliding wear behaviour as self-mated material pairs in lithiated water (PWR simulated conditions) at room and elevated temperature.

Stellite 6 (13 ± 2 vol% M_7C_3carbides) shows approximately five times more mass loss than Stellite 3 (24 ± 1 vol% M_7C_3 carbides and 18 ± 1 vol% for the η-carbide) after testing for 5 h at 250 °C in lithiated water. Both alloys show a significant increase in wear at above approximately 150–200 °C.

The main wear mechanisms are mainly similar in the two materials, both experiencing scoring, carbide pull-out and some oxide formation. The mechanisms also remain similar over the whole temperature range although Stellite 3 is more prone to local matrix removal, often associated with oxide formation.

Partial fcc to hcp phase transformation in the top 5 – 15 μm of the cobalt matrix (subsurface of the wear scar) is observed over the entire temperature range studied. The evidence suggests that in Stellite 6, the extent of transformation appears to be somewhat higher than in Stellite 3 when tested in similar conditions. This is probably due to lower carbide content of the former providing less mechanical support for the matrix.

As there is not a significant difference in either the wear mechanisms or degree of phase transformation with temperature for either

alloy, it is suggested that the marked increase in wear rate at temperatures above 150 −200 °C is mainly due to a tribocorrosion phenomenon. The significant increase in rate of material loss as the temperature is increased is caused by higher rates of corrosion layer formation at elevated temperature, combined with the repeated removal of the corrosion product from the alloy surface by the action of wear in the sliding contact.

Acknowledgements

The authors gratefully acknowledge funding from Rolls-Royce plc. This work was supported by the Engineering and Physical Sciences Research Council [grant number EP/K005138/1] United Kingdom; and the University of Nottingham. The authors thank the Nanoscale and Microscale Research Centre (nmRC) for providing access to instrumentation. Dr. Nigel Neate and Dr. Hannah Constantin are gratefully acknowledged for setting up the point source XRD measurements.

References

[1] E. Baumann, I.R. Terry, The EPR: a clear step forward in dose reduction and radiation protection, Nucl. Eng. Des. 236 (2006) 1720–1727, https://doi.org/10.1016/j.nucengdes.2006.04.011.
[2] S. Zhang, D. Zhao (Eds.), Aerospace Materials Handbook, CRC Press, Boca Raton, 2013.
[3] Deloro Wear Solutions GmbH, Technical data Stellite™ 3 alloy 1–2. 〈https://www.deloro.com/stellite-data-sheets/?Rq=stellite〉 3.
[4] Deloro Wear Solutions GmbH, Technical data Stellite™ 6 alloy 1–2. 〈https://www.deloro.com/stellite-data-sheets/?Rq=stellite〉 6.
[5] R.T. Smith, T. Lolla, D. Gandy, L. Wu, G. Faria, A.J. Ramirez, S.S. Babu, P.M. Anderson, In situ X-ray diffraction analysis of strain-induced transformations in Fe- and Co-base hardfacing alloys, Scr. Mater. 98 (2015) 60–63, https://doi.org/10.1016/j.scriptamat.2014.11.003.
[6] J. Sulley, D. Stewart, HIPed hard facings for nuclear applications - materials, key potential defects and mitigating quality control measures, 24th Int. Conf. Nucl. Eng. (2016), https://doi.org/10.1115/ICONE24-61106.
[7] P. Crook, Cobalt and Cobalt Alloys, in: ASM Handb. Vol. 2 Prop. Sel. Nonferrous Alloy. Spec. Mater., 1990, pp. 446–454.
[8] P. Crook, A.V. Levy, Friction and wear of cobalt-base wrought alloys, in: ASM Handb. Vol. 18. Frict. Lubr. Wear Technol., 10th ed., ASM International, 1992, pp. 766–771.
[9] R. Singh, D. Kumar, S.K. Mishra, S.K. Tiwari, Laser cladding of Stellite 6 on stainless steel to enhance solid particle erosion and cavitation resistance, Surf. Coat. Technol. 251 (2014) 87–97, https://doi.org/10.1016/j.surfcoat.2014.04.008.
[10] H. Yu, R. Ahmed, H. Villiers Lovelock de, H. Davies, Influence of manufacturing process and alloying element content on the tribomechanical properties of cobalt-based alloys, J. Tribol. 131 (2009), https://doi.org/10.1115/1.2991122 (011601-1-011601-011612).
[11] H. Yu, R. Ahmed, H. de Villiers Lovelock, A comparison of the tribo-mechanical properties of a wear resistant cobalt-based alloy produced by different manufacturing processes, J. Tribol. 129 (2007) 586–594, https://doi.org/10.1115/1.2736450.
[12] C. Zhao, D. Stewart, J. Jiang, F.P.E. Dunne, A comparative assessment of iron and cobalt-based hard-facing alloy deformation using HR-EBSD and HR-DIC, Acta Mater. 159 (2018) 173–186, https://doi.org/10.1016/j.actamat.2018.08.021.
[13] K.J. Bhansali, A.E. Miller, The role of stacking fault energy on galling and wear behavior, Wear 75 (1982) 241–252, https://doi.org/10.1016/0043-1648(82)90151-X.
[14] P. Crook, C.C. Li, The elevated temperature metal-to-metal wear behavior of selected hardfacing alloys, in: Wear Mater., American Society of Mechanical Engineers, 1983, pp. 272–279.
[15] F.H. Stott, C.W. Stevenson, G.C. Wood, Friction and wear properties of Stellite 31 at temperatures from 293 to 1073 K, Met. Technol. 4 (1977) 66–74.
[16] D.H.E. Persson, E. Coronel, S. Jacobson, S. Hogmark, Surface analysis of laser cladded Stellite exposed to self-mated high load dry sliding, Wear 261 (2006) 96–100, https://doi.org/10.1016/j.wear.2005.09.027.
[17] D.H.E. Persson, S. Jacobson, S. Hogmark, Antigalling and low friction properties of a laser processed Co-based material, J. Laser Appl. 15 (2003) 115–119, https://doi.org/10.2351/1.1514218.
[18] D.H.E. Persson, On the Mechanisms Behind The Tribological Performance Of Stellites, Ph.D. Thesis, Acta Universitatis Upsaliensis, 2005 ISBN 91-554-6420-3.
[19] W.H. Hocking, F.W. Stanchell, E. McAlpine, D.H. Lister, Mechanisms of corrosion of Stellite-6 on lithiated high temperature water, Corros. Sci. 25 (1985) 531–557.
[20] C. Maffiotte, M. Navas, M.L. Castaño, A.M. Lancha, XPS characterization of oxide films formed in cobalt-based alloys during corrosion tests at high temperature, Surf. Interface Anal. 30 (2000) 161–166, https://doi.org/10.1002/1096-9918(200008)30:1<161::AID-SIA764>3.0.CO;2-O.
[21] N.S. McIntyre, D. Zetaruk, E.V. Murphy, X-ray photoelectron spectroscopic study of the aqueous oxidation of Stellite-6 alloy, Surf. Interface Anal. 1 (1979) 105–110, https://doi.org/10.1149/1.2133027.
[22] N.K. Taylor, I. Armson, Corrosion product release from stellites and stainless steel in high pressure, high temperature lithiated water, in: Water Chem. Nucl. React. Syst. 3 Proceedings an International Conference, British Nuclear Society, London, 1983, pp. 141–151.
[23] W.H. Hocking, D.H. Lister, Corrosion of Stellite-6 in lithiated and borated high--temperature water, Surf. Interface Anal. 11 (1988) 45–59, https://doi.org/10.1002/sia.740110106.
[24] G.N. Karimi, P.H. Shipway, D.A. Stewart, T. Hussain, Corrosion of cast Stellite-3 analogue in simulated PWR conditions, Corros. Sci. 140 (2018) 402–411, https://doi.org/10.1016/j.corsci.2018.05.023.
[25] D. Kaczorowski, J.P. Vernot, Wear problems in nuclear industry, Tribol. Int. 39 (2006) 1286–1293, https://doi.org/10.1016/j.triboint.2006.02.048.
[26] V.-.E. Iordache, F. Wenger, P. Ponthiaux, A. Ambard, J. Peybernes, J. Vallory, Comparison between tribocorrosion mechanisms of Stellite 6 and Zircaloy 4 in LiOH-H_3BO_3 solutions, in: Passiv. Met. Semicond. Prop. Thin Oxide Layers. 2006. p. 495–500.
[27] E. Lemaire, M. Le Calvar, Evidence of tribocorrosion wear in pressurized water reactors, Wear 249 (2001) 338–344, https://doi.org/10.1016/S0043-1648(00)00544-5.
[28] S. Guadalupe Maldonado, S. Mischler, M. Cantoni, W.J. Chitty, C. Falcand, D. Hertz, Mechanical and chemical mechanisms in the tribocorrosion of a Stellite type alloy, Wear 308 (2013) 213–221, https://doi.org/10.1016/j.wear.2013.04.007.
[29] S. Xu, I.L. Kondratova, N. Arbeau, W. Cook, D.H. Lister, Corrosion of UNS R30006 in high-temperature water under intermittent mechanical contact, Corrosion 61 (2005) 444–451.
[30] V.L. Ratia, D. Zhang, M.J. Carrington, J.L. Daure, D.G. McCartney, P.H. Shipway, D.A. Stewart, The effect of temperature on sliding wear of self-mated HIPed Stellite 6 in a simulated PWR water environment, Wear 420–421 (2019) 215–225.
[31] J. Schindelin, I. Arganda-Carreras, E. Frise, V. Kaynig, M. Longair, T. Pietzsch, S. Preibisch, C. Rueden, S. Saalfeld, B. Schmid, J.Y. Tinevez, D.J. White, V. Hartenstein, K. Eliceiri, P. Tomancak, A. Cardona, Fiji: an open-source platform for biological-image analysis, Nat. Methods 9 (2012) 676–682, https://doi.org/10.1038/nmeth.2019.
[32] M.A. Ashworth, J.C. Bryar, M.H. Jacobs, S. Davies, Microstructure and property relationships in hipped Stellite powders, Powder Metall. 42 (1999) 243–249, https://doi.org/10.1179/003258999665585.
[33] H. Ocken, Performance of NOREM ™ Hardfacing Alloys TR-112993 Final Report, Electric Power Research Insitute, Palo Alto, USA, 1999.
[34] Velan Inc., EPRI NP-4993 Project 1935 Topical Report: Laboratory evaluations of cobalt-free, nickel-based hard-facing alloys for nuclear applications, Electric Power Research Insitute, Palo Alto, USA, 1987.
[35] S. Kapoor, R. Liu, X.J. Wu, M.X. Yao, Temperature-dependence of hardness and wear resistance of Stellite alloys, World Acad. Sci. Eng. Technol. 67 (2012) 964–973.
[36] K. Yamamoto, S. Inthidech, N. Sasaguri, Y. Matsubara, Influence of Mo and W on high temperature hardness of M_7C_3 carbide in high chromium white cast iron, Mater. Trans. 55 (2014) 684–689, https://doi.org/10.2320/matertrans.F-M2014801.
[37] R. Liu, X.J. Wu, S. Kapoor, M.X. Yao, R. Collier, Effects of temperature on the hardness and wear resistance of high-tungsten Stellite alloys, Metall. Mater. Trans. A Phys. Metall. Mater. Sci. 46 (2014) 587–599, https://doi.org/10.1007/s11661-014-2664-8.